The motion of small spherical particles in a cellular flow field

M. R. Maxey

Citation: Physics of Fluids (1958-1988) **30**, 1915 (1987); doi: 10.1063/1.866206
View online: http://dx.doi.org/10.1063/1.866206
View Table of Contents: http://scitation.aip.org/content/aip/journal/pof1/30/7?ver=pdfcov
Published by the AIP Publishing

The motion of small spherical particles in a cellular flow field

M. R. Maxey
Division of Applied Mathematics, Brown University, Providence, Rhode Island 02912

(Received 18 March 1986; accepted 17 March 1987)

In an earlier paper, Maxey and Corrsin [J. Atmos. Sci. **43**, 1112 (1986)] studied the motion of small aerosol particles settling under gravity through an infinite, periodic, cellular flow field subject to the effects of a Stokes drag force and inertia of the particles. Particle inertia was shown to have an important influence on the motion: No permanent suspension in the flow occurred, particles generally settled more rapidly than in still fluid, and the particle paths merged into isolated asymptotic trajectories. This study is continued for particles that are not necessarily much denser than the surrounding fluid but vary in density. Two basic responses are identified: an aerosol response for particles denser than the fluid, similar to that mentioned, and a bubble response for particles less dense. For both, particle accumulation is still a recurring feature. Results of numerical simulations are discussed, together with the stability of equilibrium points and the role of particle or fluid inertia.

I. INTRODUCTION

In an early study, Stommel[1] showed that small spherical particles may be suspended indefinitely in a cellular flow field by the action of upflow regions countering the effect of gravitational settling. The flow studied was two-dimensional, incompressible, and given by a streamfunction ψ:

$$\psi = U_0 L \sin(x_1/L)\sin(x_2/L). \tag{1}$$

Such a flow arises, for example, in thermal convection with free-slip boundaries or in Langmuir circulations. Indeed, it was in the latter context of the suspension of plankton by Langmuir cells that Stommel[1] made his study. The motion of the particles was governed by an instantaneous balance of the Stokes drag force, generated by the relative motion of the particle through the fluid, and the force due to gravity. The center $\mathbf{Y}(t)$ of a small spherical particle then moves according to

$$\begin{aligned} \frac{dY_1}{dt} &= U_0 \sin\left(\frac{Y_1}{L}\right)\cos\left(\frac{Y_2}{L}\right), \\ \frac{dY_2}{dt} &= -U_0 \cos\left(\frac{Y_1}{L}\right)\sin\left(\frac{Y_2}{L}\right) + W^{(s)}, \end{aligned} \tag{2}$$

where $W^{(s)}$ is the Stokes terminal fall velocity for still fluid. The particle velocity at any instant is the sum of the local fluid velocity and the Stokes settling velocity. The concentration of particles is low enough that they do not modify the flow field or interact with each other. Stommel[1] showed that the percentage of particles suspended in the cell depended on the ratio $W = W^{(s)}/U_0$, the nondimensional settling velocity. For $W = 0$ all particles are suspended, while for $W \geqslant 1$ no suspension occurs, with a continuous range of particles suspended for intermediate values of W.

This situation is illustrated by Fig. 1, which shows the typical streamlines and velocity profiles for the spatially periodic, cellular flow field given by (1). The maximum flow speed for each cell occurs on the cell boundaries, with stagnation points at the center and the four corners of each cell. For $W = 0$ the particles simply move with the local fluid velocity and behave as Lagrangian tracers. Since the cellular flow field is steady the particle pathlines coincide with the streamlines shown in Fig. 1. The normal component of the fluid velocity is zero on the cell boundaries, so in the absence of gravitational settling there is no tendency for particles to cross the boundaries and all particles introduced into a cell remain there indefinitely. By contrast, for $W \geqslant 1$ the Stokes settling velocity at all times dominates the fluid velocity, and the particle trajectories, found by solving (2), pass vertically from one cell to the next even though they may pass through local updraft regions. For intermediate values of W local upflow in the fluid may be sufficiently strong to cause particle suspension by the flow. Typical particle trajectories for $W = 0.5$ are shown in Fig. 2. Particles that are suspended move continuously along closed paths encircling an equilibrium point, at which a particle would be held stationary in the flow. The suspension or trapping region is bounded by a particle path that joins the cell boundary, and outside this region particles settle out, passing from one cell to the next.

A similar situation arises for buoyant particles which are then suspended in the downflow regions. In Fig. 2, as in the rest of this paper, the direction of gravitational acceleration is taken to be in the positive x_2 direction. A further

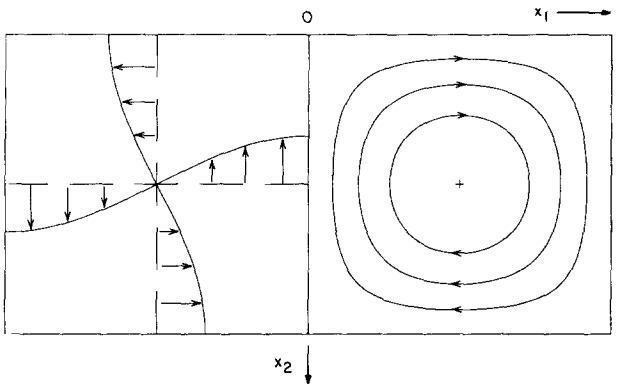

FIG. 1. Velocity profiles, shown for the left-hand cell, and streamlines, shown for the right-hand cell, for the periodic cellular flow field (1): +, stagnation point; arrows show direction of flow. Each cell is of side L.

 0031-9171/87/071915-14$01.90

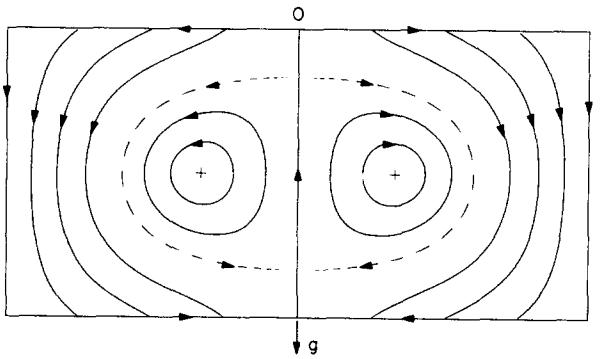

FIG. 2. Trajectories for particles without inertia settling under gravity in the cellular flow field, Eq. (2), for $W = 0.5$: +, static equilibrium point; —→—, bounding trajectory for the trapping region; ⟶, particle path. Arrows on the cell boundaries indicate the circulation in each cell.

discussion of these results and their application to crystal suspension in convecting magma chambers is given by Marsh and Maxey.[2]

In a recent paper, Maxey and Corrsin[2] have reexamined this problem for the motion of small aerosol particles for which particle inertia is significant. The equation of motion of a particle is then

$$m_p \frac{d\mathbf{V}}{dt} = 6\pi a\mu[\mathbf{u}(\mathbf{Y}(t),t) - \mathbf{V}(t)] + m_p\mathbf{g}, \tag{3}$$

where m_p is the particle mass, a is the particle radius, $\mathbf{V}$ is the particle velocity, μ is the viscosity of the surrounding fluid, and $\mathbf{g}$ is the acceleration due to gravity. The fluid velocity is $\mathbf{u}(\mathbf{x},t)$. There is now, in addition to the dimensionless Stokes settling velocity

$$W = W^{(s)}/U_0 = m_p g/6\pi a\mu U_0, \tag{4}$$

another dimensionless parameter $1/A$, sometimes referred to as the Stokes number, which measures the dimensionless response time of the particle motion to changes in the velocity of the surrounding fluid. The parameter A is defined by

$$A = 6\pi a\mu L/m_p U_0 \tag{5}$$

and determines specifically how important particle inertia is, with inertia more significant the smaller the value of A. The main conclusions of this study were that for all finite values of A no particle is suspended indefinitely if W is nonzero, and that all particles eventually settle out under gravity, with an average settling velocity generally greater than $W^{(s)}$. It was also found, somewhat surprisingly, that for weak or moderate inertia, when A is not small, all the particles eventually collected along well-defined accumulation curves, with the individual particle trajectories merging into isolated asymptotic paths. These paths had a periodic structure and passed primarily through the downflow region of each cell, leading to the observed increase in effective settling velocity.

The purpose of this paper is to consider the motion of a general, small, spherical particle that is not necessarily much denser than the surrounding fluid and to examine whether this type of motion persists in a more general context. In the following sections the results of some numerical simulations are described for spherical particles as they move in response to a periodic cellular flow field, as given by (1). Attention will be focused on how the character of the particle motion changes with variations in the relative density of the particle to the fluid. Two limiting cases will be discussed: the aerosol limit, where the particle density is much greater than the fluid density; and the bubble limit, where the particle density is negligible.

Some related studies have been reported previously by Wood and Jenkins[4] for particles in a cellular flow field, by Manton[5] and Nielsen[6] for particles in various vortex flow fields, and by Auton[7] and Thomas *et al.*[8] for bubbles in a vortex flow. Wood and Jenkins[4] computed a limited number of particle trajectories for particles settling in water and included in their equation of particle motion fluid drag forces that depended nonlinearly on the relative velocity of the particle to the fluid and various fluid inertia effects such as added mass. Wood and Jenkins[4] noted particle suspension in some instances, but in others found particles settling faster than in still fluid. The approach of both Manton[5] and Nielsen[6] was to assume that (2) held as a first approximation, i.e., the particle velocity is the sum of the local fluid velocity and the settling velocity for still fluid, and to then include inertial terms or other terms as small corrections. Manton[5] analyzed the linear stability of the equilibrium suspension points where the local, upward, fluid velocity holds a particle stationary against gravitational settling. Manton found that for both a potential line vortex or a uniform vorticity distribution these points were unstable. Nielsen[6] found similar results, but also found that the equilibrium points become stable if the particle is less dense than the surrounding fluid. This result also agrees with Auton's[7] observation that for bubbles the equilibrium point in a line vortex flow is stable, and that for a region around this point the bubbles spiral in toward it and are trapped.

In the cellular flow field the equilibrium points are unstable for aerosol particles with inertia, as in (3), and correspondingly no permanent particle suspension was found. The stability or otherwise of these points provides an indication of whether or not particle suspension may occur. The question of the linear stability of the equilibrium points is discussed in Sec. III. A simplified explanation of these changes in stability characteristics, though, can be given in terms of the opposing roles of particle inertia and added mass or fluid acceleration effects. In the examples mentioned above and in the cellular flow field context a particle subject only to gravitational settling and fluid drag forces, but with negligible inertia, may be suspended at an equilibrium point in the flow. If displaced slightly the particle will move along a simple closed path, encircling the equilibrium points, similar to the paths shown in Fig. 2. An aerosol particle with particle inertia will not follow such a closed path, but will tend to spiral outward due to its inertia. The effects of added mass of the particle and fluid acceleration act in the opposite sense to particle inertia, so that a buoyant particle, for which these effects dominate particle inertia, will tend to spiral inward back toward the equilibrium point.

In Sec. II we give a statement of the equation of particle motion to be used and define the nondimensional parameters. In Secs. III–VI, the numerical results from simulations of the particle motions are described.

II. EQUATION OF PARTICLE MOTION

The equation of motion for a small rigid sphere in a nonuniform or unsteady flow field under general conditions[9] is

$$m_p\frac{d\mathbf{V}}{dt} = (m_p - m_F)\mathbf{g} + m_F\frac{D\mathbf{u}}{Dt}\bigg|_{\mathbf{Y}(t)} - \frac{1}{2}m_F\frac{d}{dt}\left(\mathbf{V} - \mathbf{u}(\mathbf{Y},t) - \frac{1}{10}a^2\nabla^2\mathbf{u}\right) - 6\pi a\mu\mathbf{X}(t) - 6\pi a^2\mu\int_0^t d\tau\frac{d\mathbf{X}/d\tau}{\sqrt{\pi\nu(t-\tau)}}, \quad (6)$$

where

$$\mathbf{X}(t) = \mathbf{V}(t) - \mathbf{u}(\mathbf{Y}(t),t) - \tfrac{1}{6}a^2\nabla^2\mathbf{u} \quad (7)$$

and in addition to previously defined terms m_F is the mass of the displaced fluid and ν is the kinematic viscosity of the surrounding fluid. The term in $D\mathbf{u}/Dt$ is the fluid element acceleration at the instantaneous position of the particle and represents the fluid force on the particle from the undisturbed flow field. Otherwise, time derivatives are taken following a particle trajectory. Also included in (6) are the buoyancy force of the fluid on the particle, the added mass effect, the Stokes drag law, the Basset history term, and Faxen corrections for the nonuniform flow field. Equation (6) is applicable to small particles at low Reynolds numbers provided that

$$a/L \ll 1,\ aW^{(s)}/\nu \ll 1,\ a^2U_0/L\nu \ll 1, \quad (8)$$

based on the scales U_0 and L for the cellular flow field.

The inclusion of the Basset history term in the form given in (6) further requires that the initial particle velocity $\mathbf{V}(t=0)$ be given by the condition that $\mathbf{X}(t=0)$ defined by (7) vanishes, namely,

$$\mathbf{V}(t=0) = \mathbf{u}(\mathbf{Y}(0),0) + \tfrac{1}{6}a^2\nabla^2\mathbf{u}. \quad (9)$$

Other particle velocity conditions can be included provided the Basset history term is modified accordingly.

Equation (6) as it stands is quite complicated and a simplified equation of motion will be considered instead, where the Basset history term is neglected and the Faxen corrections are omitted. For the steady cellular flow field (1) the Faxen corrections simplify as

$$a^2\nabla^2\mathbf{u} = -2a^2\mathbf{u}/L^2 \quad (10)$$

and their effect in (6) is equivalent to decreasing by a very small amount the local value of $\mathbf{u}(\mathbf{Y},t)$. This is unlikely to have any significant result on the general particle motion and will not be considered further. The Basset history term may also be neglected as a first approximation. The primary focus here is on the effect of a small but finite degree of inertia on the particle motion; indeed, the restrictions (8) require that the effects of fluid inertia be small. If the inertia terms are neglected altogether, (6) reduces to a quasisteady balance of gravitational forces with the Stokes drag force and then $\mathbf{X}(t)$ is simply a constant. If corrections for inertia are included it may be shown[5] that the Basset history term is less significant than the other terms. Test computations with the Basset term included showed that it only had a minor effect on the results presented here. It is neglected in the present treatment. The simplified equation of motion for particles in the steady cellular flow field is

$$\left(m_p + \frac{1}{2}m_F\right)\frac{d\mathbf{V}}{dt} = (m_p - m_F)\mathbf{g} + 6\pi a\mu[\mathbf{u}(\mathbf{Y},t) - \mathbf{V}(t)] + m_F\mathbf{u}\cdot\nabla\mathbf{u} + \tfrac{1}{2}m_F\mathbf{V}\cdot\nabla\mathbf{u}, \quad (11)$$

which differs from Eq. (3) for an aerosol particle by the inclusion of terms in m_F.

One of the principle aims of this study is to see how the particle motion changes as the ratio of particle to fluid densities, or equivalently the ratio of the masses m_p and m_F, is varied. The ratio m_p/m_F may vary between zero and infinity; it is useful to divide this into the two ranges, corresponding to two different sets of physical conditions. The first of these is the aerosol range where the particle density remains significantly greater than the fluid density, and which specifically covers the range $m_p \geqslant 2m_F$. Here the fluid acceleration and added mass terms of (11) are regarded as small perturbations to the basic aerosol problem. The mass of the particle, or rather $(m_p + \frac{1}{2}m_F)$, is taken as the reference value and the simplified equation of motion (11) is rewritten as

$$\frac{d\mathbf{V}}{dt} = \alpha[\mathbf{u}(\mathbf{Y},t) + \mathbf{W}^{(s)} - \mathbf{V}(t)] + R\left(\mathbf{u} + \frac{1}{2}\mathbf{V}\right)\cdot\nabla\mathbf{u}, \quad (12)$$

where

$$\alpha = 6\pi a\mu/(m_p + \tfrac{1}{2}m_F), \quad (13)$$

$$R = m_F/(m_p + \tfrac{1}{2}m_F), \quad (14)$$

and the Stokes settling velocity $\mathbf{W}^{(s)}$ for still fluid is

$$\mathbf{W}^{(s)} = (m_p - m_F)\mathbf{g}/6\pi a\mu. \quad (15)$$

The equation of motion is scaled by U_0, the maximum flow speed in the cell and by L, the size of the cell as given by (1). Nondimensional variables are introduced as follows:

$$\mathbf{x}^* = \frac{\mathbf{x}}{L},\quad \mathbf{Y}^* = \frac{\mathbf{Y}}{L},\quad t^* = \frac{tU_0}{L},\quad \mathbf{V}^* = \frac{\mathbf{V}}{U_0},\quad \mathbf{u}^* = \frac{\mathbf{u}}{U_0}.$$

The scaled form of (12), with the asterisks suppressed, is

$$\frac{d\mathbf{V}}{dt} = A[\mathbf{u}(\mathbf{Y},t) + \mathbf{W} - \mathbf{V}(t)] + R\left(\mathbf{u} + \frac{1}{2}\mathbf{V}\right)\cdot\nabla\mathbf{u}. \quad (16)$$

The nondimensional parameters characterizing the particle motion are the inertia parameter A now defined as

$$A = \alpha L/U_0 \quad (17)$$

and the scaled particle settling velocity for still-fluid W defined as

$$\mathbf{W} = \mathbf{W}^{(s)}/U_0. \quad (18)$$

These definitions agree with those given previously in (4) and (5) when the density of the surrounding fluid is neglected and m_F is zero.

In the aerosol range we consider the effect of varying the mass ratio parameter R while keeping A and W fixed. The mass ratio R is zero for an aerosol system, where m_F is zero, and increases continuously to a value of 0.4 when the ratio m_p/m_F equals 2. For R equal to zero the scaled equation of particle motion (16) is the same as for the aerosol system considered by Maxey and Corrsin.[3] Thus by varying the val-

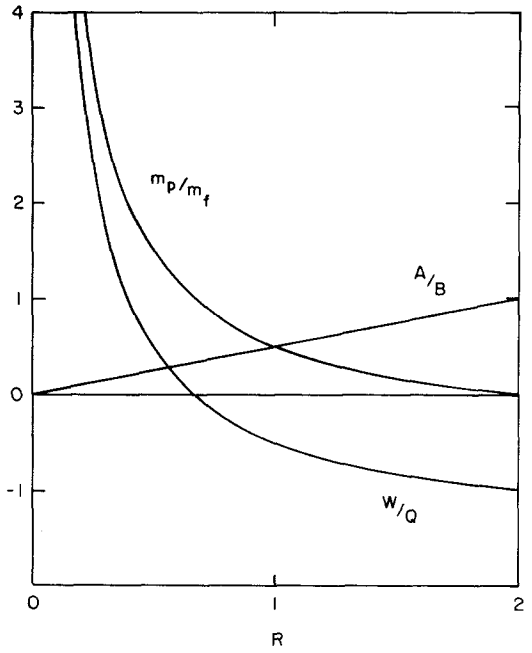

FIG. 3. Variations of W, A, and m_p/m_F for fixed values of Q and B with changing values of the mass ratio parameter R: Curves for A/B, W/Q, m_p/m_F are as marked.

ue of the mass ratio R a direct connection with the study in Ref. 3 for aerosol particles can be made and the effect of limited added mass and fluid acceleration effects can be investigated. In a physical experiment these conditions can be achieved by varying the density of the fluid and the scales U_0 and L of the flow field while keeping the size of the particle and its mass fixed. Thus in the aerosol range the particle properties are regarded as fixed, while the flow conditions in the surrounding fluid are varied in such a way as to maintain constant values of A and W. The results of the study in Ref. 3 show that the parameters A and W are the most natural to use: Indeed, we find that whether or not particle suspension can occur depends directly on the value of W, the ratio of still-fluid settling velocity to the maximum upflow of U_0, rather than some other velocity scale.

While these parameters are well suited to the aerosol problem, they are not convenient for the second range, which covers particle masses m_p between zero and $2m_F$. This range includes both the bubble limit, where the particle is a vapor bubble of negligible mass and the transition range, where the particle changes from being more dense to less dense than the surrounding fluid. A particle of the same density as the fluid is neutrally buoyant and has zero settling velocity. Furthermore, as the particle density decreases the particle ceases to settle under gravity, but instead rises due to buoyancy forces. It is no longer appropriate to regard the dimensionless settling velocity W as fixed; some other scaling that takes account of the changes in relative density is needed. The physical context that is considered in this second range is one in which the fluid properties, flow speed, and length scales are fixed, but the mass of the particle m_p varies. We thus investigate the motion of particles of a fixed size, but varying density, in a given cellular flow field.

This second range, which covers $0 \leqslant m_p/m_F \leqslant 2$, is referred to here as the bubble range. A spherical bubble of radius a and negligible particle mass $m_p = 0$ rises vertically in still fluid at a terminal velocity

$$\mathbf{W}^{(s)} = -m_F \mathbf{g}/6\pi a\mu, \tag{19}$$

as given by (15). This is calculated from the Stokes drag law for a rigid particle, but this is also a good approximation[10] for small vapor bubbles in the presence of surface impurities. Other appropriate forms of the Stokes law may be incorporated as desired. The nondimensional speed, scaled by U_0, at which such a bubble will rise in still fluid is

$$Q = |\mathbf{W}| = m_F g/6\pi a\mu U_0. \tag{20}$$

This bubble rise speed Q will be used as the reference value for the bubble range. Similarly, the inertia parameter A for a vapor bubble will be used as the reference value, namely,

$$B = 6\pi a\mu L/(\tfrac{1}{2} m_F U_0), \tag{21}$$

based on (13) and (17) for m_p equal to zero.

As the relative densities of the particle and fluid vary over the bubble range the values of B and Q will be regarded as the fixed parameters. The actual values of the settling velocity parameter W and inertia parameter A will change with changes in the ratio m_p/m_F. These changes are specified in terms of the mass ratio parameter R, defined by (14), as

$$W = [(m_p - m_F)/m_F]Q = (1/R - \tfrac{3}{2})Q, \tag{22}$$

$$A = RB/2 \tag{23}$$

and the ratio m_p/m_F is related to the mass ratio parameter R by

$$m_p/m_F = 1/R - \tfrac{1}{2}. \tag{24}$$

Over the bubble range the parameter R increases continuously from a value of 0.4 when $m_p = 2m_F$ to a value of 2.0 when $m_p = 0$ in the bubble limit. When the particle is neutrally buoyant and $m_p = m_F$ then R has a value of $\frac{2}{3}$. Figure 3 shows how W, A, and m_p/m_F vary with different values of the mass ratio parameter R for fixed values of Q and B. Note that W is positive for $R < \frac{2}{3}$ and negative for $R > \frac{2}{3}$, corresponding to the transition from a denser particle that settles downward to a buoyant particle that rises upward in still fluid.

The equations of particle motion for particles in the cellular flow field (1) are, from (16),

$$\frac{1}{A}\frac{dV_1}{dt} + V_1 = \sin Y_1 \cos Y_2 + \frac{1}{2}\frac{R}{A}(V_1 \cos Y_1 \cos Y_2 - V_2 \sin Y_1 \sin Y_2) + \frac{R}{A}\sin Y_1 \cos Y_1, \tag{25a}$$

$$\frac{1}{A}\frac{dV_2}{dt} + V_2 = -\cos Y_1 \sin Y_2 + W + \frac{1}{2}\frac{R}{A}(V_1 \sin Y_1 \sin Y_2 - V_2 \cos Y_1 \cos Y_2) + \frac{R}{A}\sin Y_2 \cos Y_2. \tag{25b}$$

Solutions to Eqs. (25) may be computed with suitable choices for the initial particle position and velocity.

III. EQUILIBRIUM POINTS AND STABILITY

The existence or not of equilibrium points for the particles has been alluded to in Secs. I and II; this question has an important bearing on the general features of the particle motion. A linear stability analysis of these points further provides an indication of whether or not particle suspension will occur. A particle will be held stationary by the flow if the net force on the particle vanishes. Based on the equations of motion as given by (25), an equilibrium point (Y_1^0, Y_2^0) must satisfy the conditions

$$0 = \sin Y_1^0 \cos Y_2^0 + R/A \sin Y_1^0 \cos Y_1^0, \tag{26}$$

$$0 = W - \cos Y_1^0 \sin Y_2^0 + R/A \sin Y_2^0 \cos Y_2^0. \tag{27}$$

Equilibrium is determined by the value of W and the value of R/A, which from (23) is also equal to $2/B$, with B the inertia parameter for a bubble. Equilibrium points may be found on the vertical cell boundaries where $\sin Y_1^0$ vanishes. For example, for $Y_1^0 = 0$, (26) is immediately satisfied and static equilibrium points at Y_2^0 are specified by solutions to

$$W = \sin Y_2^0 - R/A \cos Y_2^0 \sin Y_2^0, \tag{28}$$

where these exist. When R is zero these equilibrium points occur where Y_2^0 is equal to $\sin^{-1}(W)$.

Equilibrium points also exist within the interior of each cell provided W is small enough. Here $\sin Y_1^0$ is nonzero and may be cancelled from (26), which leads, after elimination of $\cos Y_1^0$ from (27), to the conditions

$$\sin 2Y_2^0 = -2W(R/A)/(1 + R^2/A^2), \tag{29}$$

$$\cos Y_1^0 = W/[(1 + R^2/A^2)\sin Y_2^0]. \tag{30}$$

Solutions of (29) and (30) are chosen so that as $R \to 0$, $Y_2^0 \to \pi/2$. These results apply to particles denser than the fluid, in which case W is positive and the equilibrium point lies in the range $0 \leqslant Y_1^0 \leqslant \pi/2$, $\pi/2 \leqslant Y_2^0 \leqslant \pi$; or to particles less dense than the fluid, with W negative and $\pi/2 \leqslant Y_1^0 \leqslant \pi$, $0 \leqslant Y_2^0 \leqslant \pi/2$. Equilibrium points exist for $A/R \geqslant \sqrt{2}$ if

$$|W| \leqslant (1 + R^2/A^2)(1 - R^2/A^2)^{1/2}, \tag{31}$$

or for $A/R < \sqrt{2}$ if

$$|W| \leqslant \tfrac{1}{2}(A/R + R/A). \tag{32}$$

The stability of these equilibrium points may be determined by a linearization of the equations of particle motion (25) about the static equilibrium point (Y_1^0, Y_2^0). The linearized equations have solutions proportional to $\exp(\lambda t)$ and the possible values of λ are the roots of the quartic polynomial

$$\lambda^4 + 2A\lambda^3 + K_3\lambda^2 + K_4\lambda + K_5 = 0, \tag{33}$$

where

$$K_3 = A^2 - Rc_1 + \tfrac{1}{4}R^2 c_2, \tag{34a}$$

$$K_4 = ARc_2 - ARc_1 + \tfrac{1}{2}R^2 c_3, \tag{34b}$$

$$K_5 = A^2 c_2 + ARc_3 + R^2 \cos 2Y_1^0 \cos 2Y_2^0, \tag{34c}$$

$$c_1 = \cos 2Y_1^0 + \cos 2Y_2^0, \tag{34d}$$

$$c_2 = \sin^2 Y_1^0 \sin^2 Y_2^0 - \cos^2 Y_1^0 \cos^2 Y_2^0, \tag{34e}$$

$$c_3 = \cos Y_1^0 \cos Y_2^0 (\cos 2Y_2^0 - \cos 2Y_1^0). \tag{34f}$$

In general the roots of the polynomial (33) must be found numerically, but some special results may be deduced.

In the aerosol limit $R = 0$, the coefficients (34) simplify considerably and explicit expressions for λ can be found. For points on the cell boundary, $Y_1^0 = 0$ and $W < 1$, there is one positive real root. When $W = 1$ the equilibrium points on the cell boundary and the internal equilibrium points merge at (Y_1^0, Y_2^0) equal to $(0, \pi/2)$. The roots are then $\lambda = 0$ or $\lambda = -A$ and the point is neutrally stable. The roots for the internal equilibrium points for $W < 1$ form two complex conjugate pairs

$$\lambda = r \pm ib, \quad \lambda = s \pm ib, \tag{35}$$

where

$$rs = -b^2, \tag{36a}$$

$$r + s = -A. \tag{36b}$$

At least one or the other of r and s must be positive in order to satisfy (36a), and so this point is unstable.

Numerical evaluations show that in general the equilibrium points on the cell boundaries are unstable for all values of R. At certain values of W the growth rates of these instabilities are small. A particle passing close to such a point may appear to be temporarily suspended in the flow, as found in the simulation results of Sec. IV. With $R = 0.4$ and $A = 2$, the growth rate λ has a minimum positive value of $O(10^{-2})$ at $W = 1.019$. Within the aerosol range $0 \leqslant R \leqslant 0.4$, the internal equilibrium points were found to be unstable over the entire range. This is consistent with the observed lack of particle suspension.

As the mass ratio parameter R increases, approaching the bubble limit of $R = 2$, stable equilibrium points may be found in the interior of each cell. Within the range $0.4 \leqslant R \leqslant 2$ it is appropriate to use the "bubble range" parameters introduced in Sec. II and the parameters B and Q instead of A and W. Figure 4 shows the stability boundary as a function of R for $B = 10$. At $R = 2$, the bubble limit, equilibrium points exist if the still-fluid, bubble rise speed Q is less than 1.019. However, the point is stable only if Q is less than 1.00. As R decreases from 2 the maximum values of Q for stability and for existence of equilibrium both increase, with the latter being greater. As R approaches $\frac{2}{3}$ both tend to infinity.

The same stability boundary can be given in terms of W, which is also shown in Fig. 4. The values of W and Q are related by (22) and as R passes through the value of $\frac{2}{3}$, corresponding to a neutrally buoyant particle, W goes to zero and changes sign for any fixed value of Q. Equilibrium is possible if $|W| \leqslant 1.019$ independent of R, while stability, for some range of W, is only possible if R is greater than $\frac{2}{3}$, i.e., if the particle is less dense than the surrounding fluid. In fact, the transition between instability and possible stability will in all cases occur when $R = \frac{2}{3}$ and the particle is neutrally buoyant. This may be seen by examining the stability polynomial (33) for $W = 0$ and $R = \frac{2}{3}$. The equilibrium point then lies at the center of the cell at the stagnation point $Y_1^0 = \pi/2$ and $Y_2^0 = \pi/2$ from (29) and (30). The roots of the polynomial are $\lambda = \pm i$ and a pair of conjugate complex roots, both with negative real parts. As R increases through the value of $\frac{2}{3}$ all the roots correspond to stable solutions. In any physical situation the value of Q is finite and the still-fluid settling velocity W will pass through zero at this point, $R = \frac{2}{3}$. Hence the

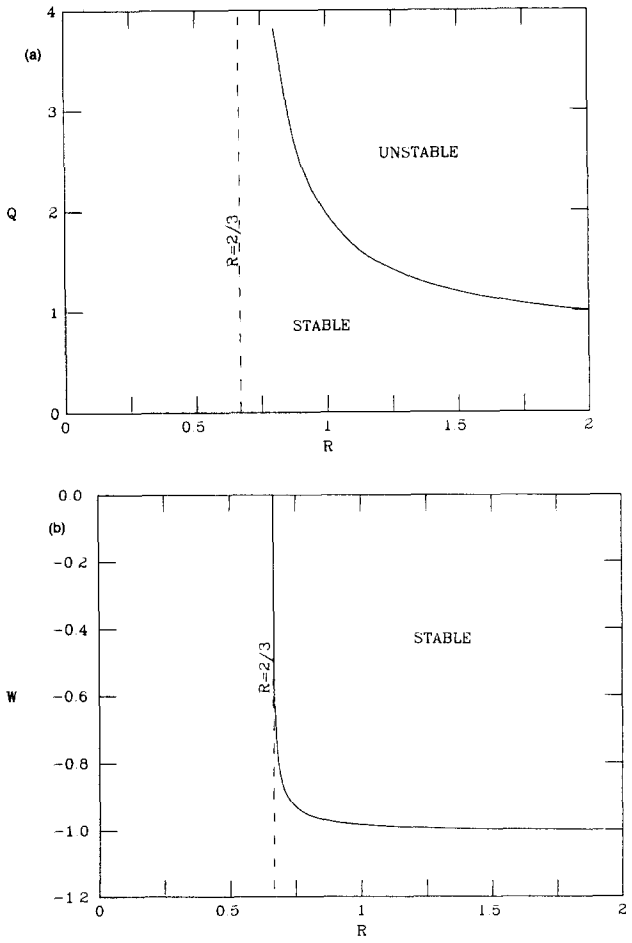

FIG. 4. Stability diagram for the particle equilibrium points in the interior of each cell as the mass ratio parameter R is varied and as W or Q are varied. Note that Q and W are related by (22). The inertia parameter $B = 10.0$.

stability transition will always occur at $R = \frac{2}{3}$ irrespective of the value of Q or B.

These observations about particle stability agree with the results found in other flow fields for similar equations of particle motion. As discussed in Sec. I, Nielsen[6] found that particle equilibrium points became stable as the density of the particle decreased below that of the surrounding field. Manton[5] found the equilibrium points for aerosol particles to be unstable, while Auton[7] found them to be stable for bubbles. Further, these results quantify the simplified explanation for the change in stability properties noted in Sec. I. This change in behavior as the particle changes from being more dense to less dense than the surrounding fluid is discussed further in Sec. VII.

IV. AEROSOL RANGE: $R \ll 0.4$

Numerical solutions for the general motion of an aerosol particle may be computed from the equations of motion (25). Since the Basset history term is not included there is no specific initial condition on the particle velocity. For convenience the initial particle velocity has been taken here to be zero. The motion of the particles is not sensitive to the choice of the initial velocity, especially if attention is focused on the long-term characteristics of the motion.

Some sample particle trajectories for aerosol particles $R = 0$ are shown in Fig. 5, with dimensionless still-fluid settling velocity $W = 0.5$ and inertia parameter $A = 5$. Five different particle trajectories are shown, none of which are closed or show particle suspension even though several of them originate in the upflow regions of the cells. This may be contrasted with Fig. 2, where there is no particle inertia and where a significant proportion of the particles are suspended. A general feature for finite values of the inertia parameter A is that particle suspension does not occur and that all particles eventually settle out under gravity. A stability analysis for the equilibrium points within each cell, as shown in Fig. 2, shows that these points are unstable for $A < \infty$. Another feature of the particle motion that is evident in Fig. 5 is the tendency for the trajectories to merge into isolated asymptotic paths. Two trajectories have actually merged, while two others in different cells have developed the same form. This, too, is a general feature for the motion of aerosol particles with inertia, as reported previously.[3]

A useful way to view the motion of the particles is to follow the paths of an array of particles initially distributed uniformly throughout the cellular flow field. Then at subsequent times the positions are plotted for all particles that lie within a selected set of cells. Here the four adjoining cells $0 \leqslant Y_1, Y_2 \leqslant 2\pi$ are used. These particle position diagrams show any tendency the particles may have to accumulate locally in parts of the flow field. The required trajectories are obtained by releasing $2N^2$ particles, at $t = 0$, with initial positions

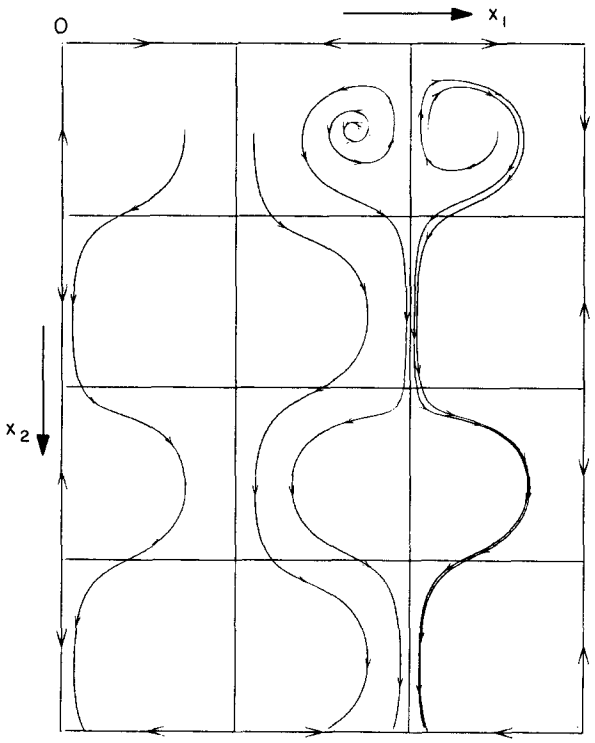

FIG. 5. Trajectories for aerosol ($R = 0$) particles settling under gravity in the cellular flow field, Eq. (25), for $W = 0.5$ and $A = 5$. Particles start from rest, and initial positions $(Y_1(0)/\pi, Y_2(0)/\pi)$ are (0.7,0.5), (1.1,0.5), (1.7,0.5), (2.1,0.5), and (2.5,0.5). Arrows on trajectories are drawn at intervals $\Delta t = 2.0$; arrows on the cell boundaries indicate the circulation in the adjoining cell.

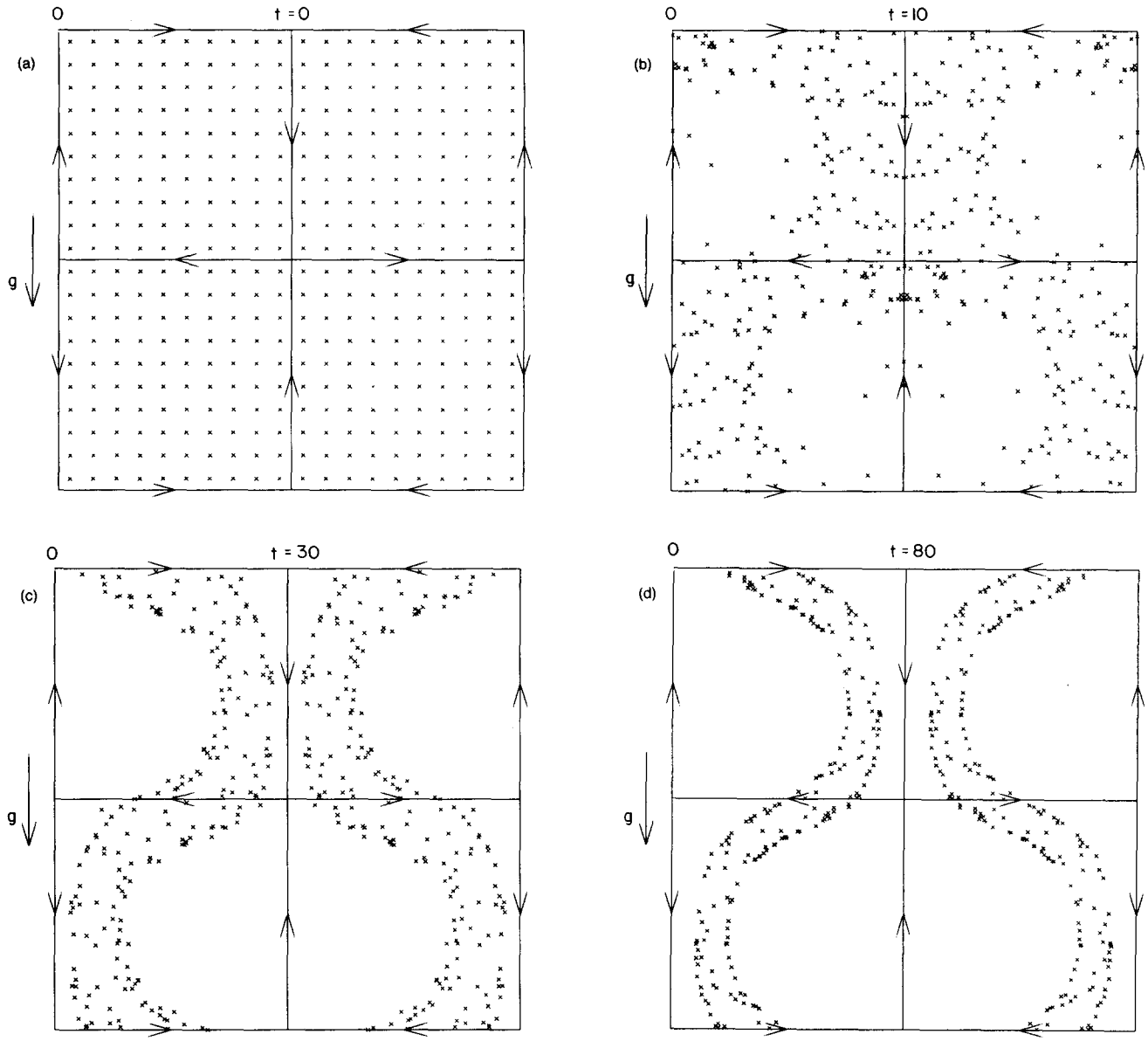

FIG. 6. Time sequence of particle position plots for aerosol ($R = 0$) particles settling under gravity for $W = 0.5$ and $A = 5$: (a) $t = 0$; (b) $t = 10$; (c) $t = 30$; (d) $t = 80$. Particle positions are marked x; arrows on the cell boundaries indicate the circulation in each cell; gravity acts in the positive x_2 direction.

$$(Y_1(t=0), Y_2(t=0)) = ((n_1 - \tfrac{1}{2})\pi/N, (n_2 - \tfrac{1}{2})\pi/N), \tag{37}$$

where $n_1 = 1,2,...,2N$ and $n_2 = 1,2,...,N$. These trajectories are extended using the periodic nature of the flow field to give the trajectories of other particles in this infinite array. It is simple to verify that if $(Y_1(t), Y_2(t))$ is a particle trajectory, so also are $(Y_1(t) + \pi, Y_2(t) + \pi)$ and $(Y_1(t) + 2m_1\pi, Y_2(t) + 2m_2\pi)$ for any integers m_1 and m_2. Typically a value of $N = 10$ has been used. The particle position diagrams are generated by computing the $2N^2$ trajectories specified by (37) and then reducing them through the periodicity conditions to give the positions within the four cells.

A time sequence of these position plots is shown in Fig. 6, again for $A = 5$ and $W = 0.5$. After the particles are released a void develops in the upflow region of each cell, where particles would have been suspended in the absence of inertia. The particles then proceed to collect within a band $t = 30$ and eventually accumulate on well-defined, isolated curves which remain the same at all subsequent times. These position plots confirm the observation that all the particles eventually settle out. Further, since these accumulation curves are asymptotically stationary this means that the individual particles must remain on them at all times and move along them. These curves thus correspond to segments of some asymptotic particle trajectory, into which the neighboring trajectories merge. Two distinct curves exist in each cell, both curves are periodic in the x_2 direction, and both curves repeat every two cells. This corresponds to two distinct asymptotic trajectories that pass through each cell; these trajectories are periodic in x_2. The two curves are not independent, though, since one may be obtained from the other by a displacement of one cell in the x_2 direction and a reflection about $x_1 = \pi$.

Other particle position plots are shown in Fig. 7. In the absence of particle inertia there is no tendency for particles

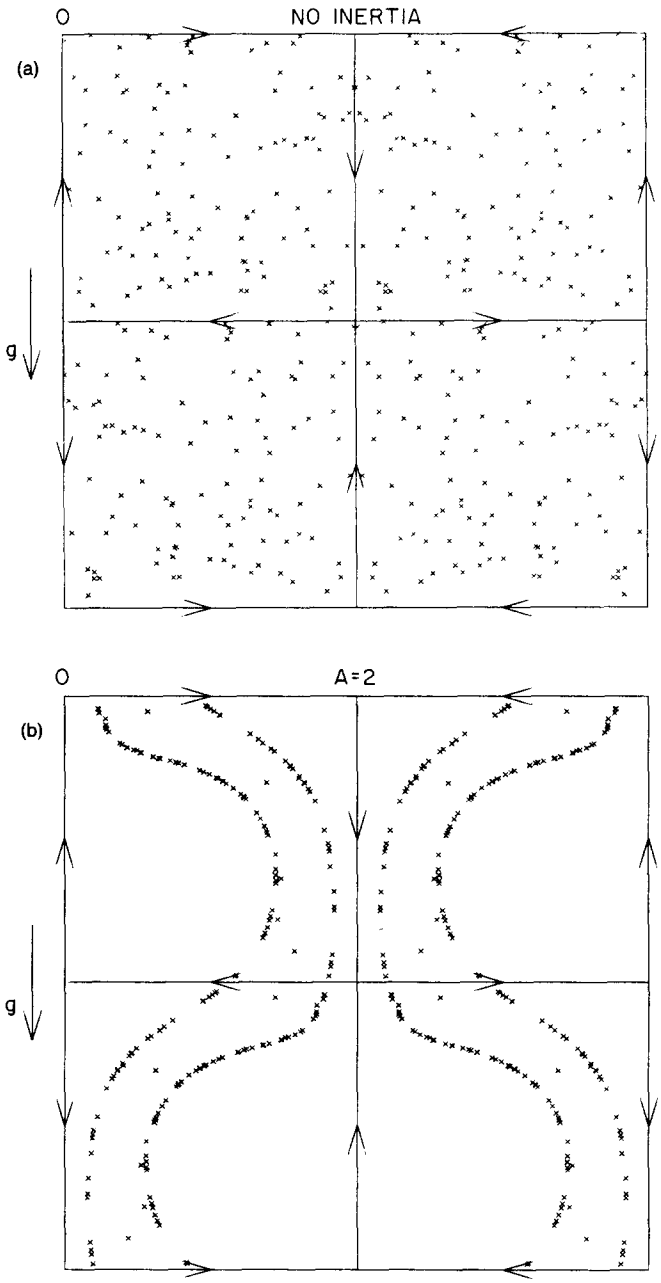

FIG. 7. Particle position plots of aerosol particles, $R = 0$, at $t = 40$ for $W = 0.5$: (a) no inertia, A is infinite; (b) particles with inertia, $A = 2$.

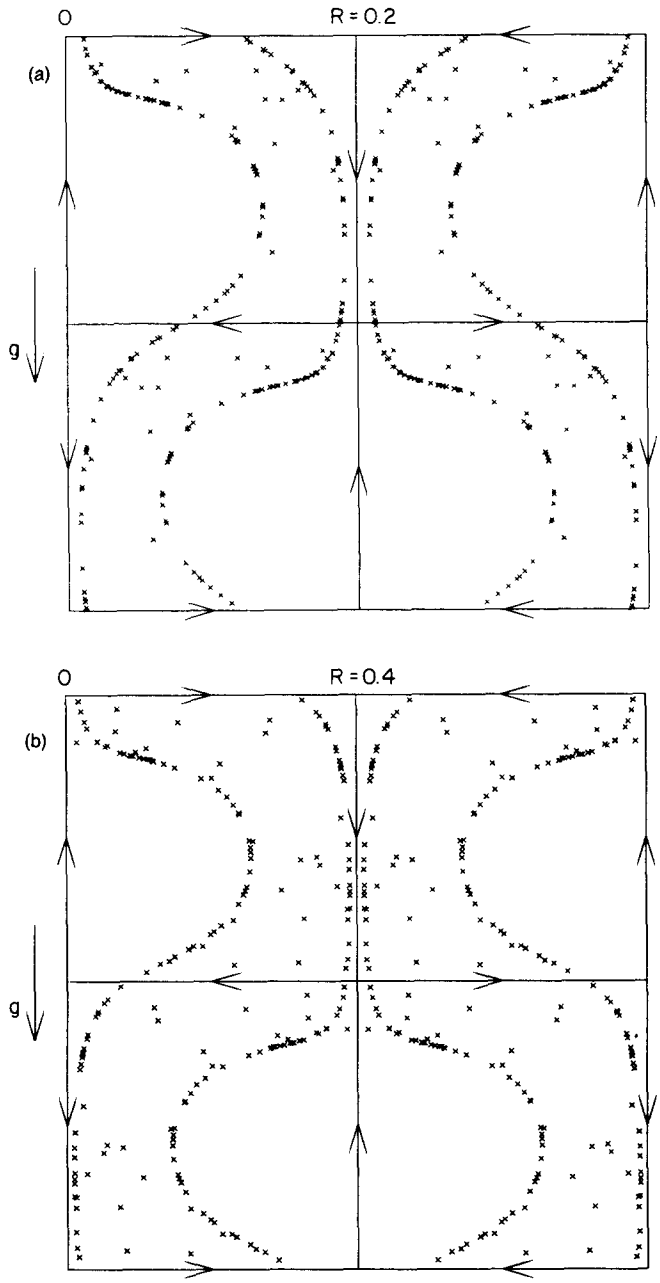

FIG. 8. Particle position plots at $t = 40$ for nondimensional settling velocity $W = 0.5$ and inertia parameter $A = 2.0$: (a) mass ratio parameter $R = 0.2$; (b) $R = 0.4$.

to accumulate and particles remain scattered throughout each cell. The individual particle trajectories are distinct, but are either closed or periodic in x_2, as illustrated by Fig. 2. For $A = 2$ the particles accumulate in much the same way as for $A = 5$ and the trajectories eventually merge into isolated asymptotic paths. Particle position plots thus provide not only information about local accumulations of particles, but also show whether or not the trajectories merge, and if they do the plots give the structure of the asymptotic trajectories.

When the mass ratio parameter R is nonzero the particle trajectories show very similar features to those of the aerosol particles $R = 0$. As R varies between 0 and 0.4 there are few significant differences: All particles eventually settle out under gravity and the trajectories in general merge into asymptotic paths. For example, position plots for $R = 0.2$ and $R = 0.4$ are shown in Fig. 8, and these are much the same as for $R = 0$ shown in Fig. 7(b). For still-fluid settling velocities W greater than about 1, particle suspension is impossible even in the absence of inertia. When $R = 0$, the particle trajectories merge and asymptotically the particles settle out along the vertical cell boundaries. Some sample trajectories in Fig. 9 for $W = 1.25$ illustrate this process. After falling through four cells all but one of the original nine trajectoreis have collected along the cell boundaries. When R equals 0.4, the same process takes place, but takes longer to become established.

As the still-fluid settling velocity W is increased further there is a difference in the motions for $R = 0$ and $R = 0.4$.

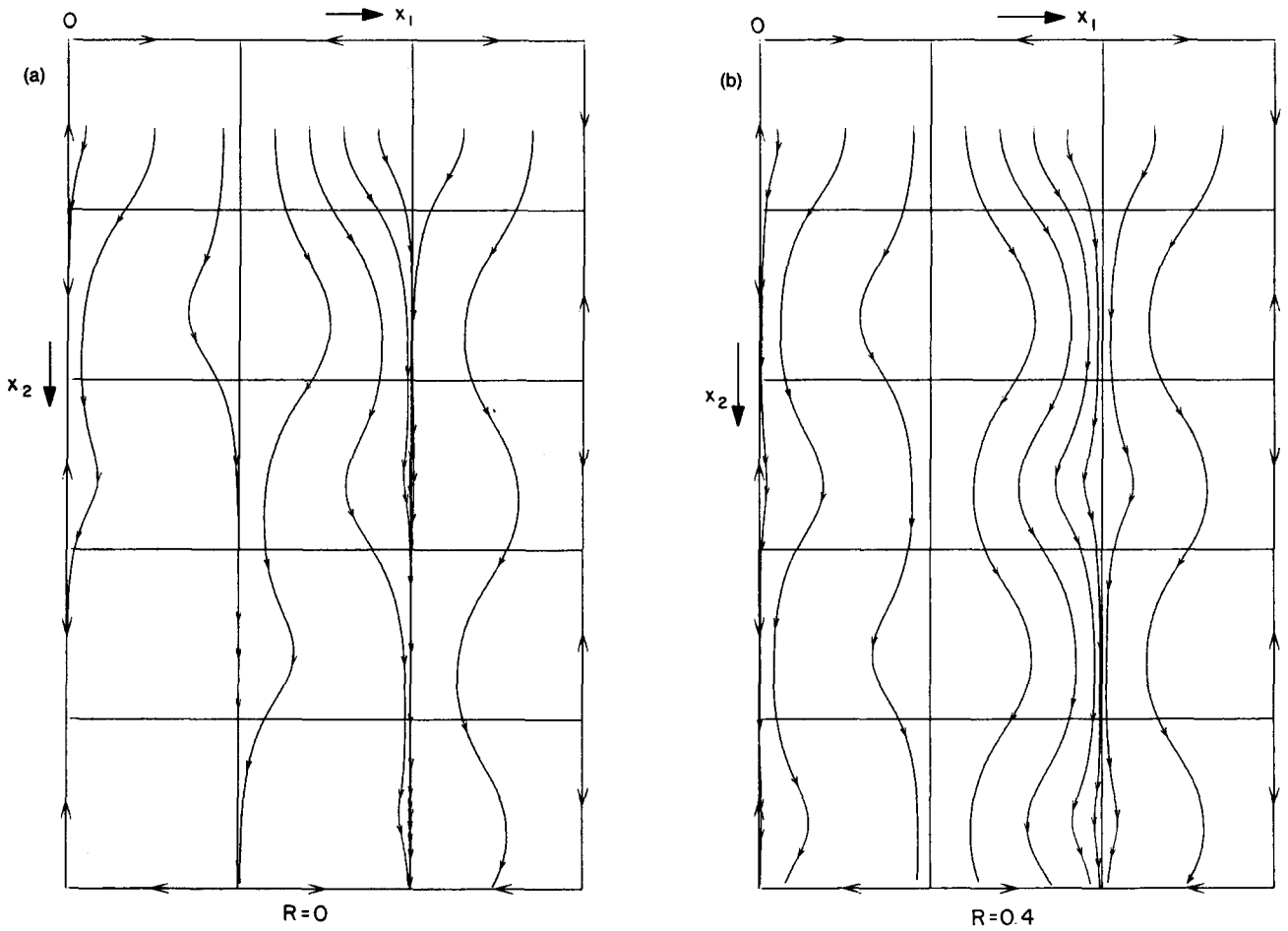

FIG. 9. Trajectories for particles settling under gravity with $W = 1.25$ and $A = 2$: (a) mass ratio parameter $R = 0$; (b) $R = 0.4$. Initial particle positions are $Y_1(0)/\pi = 0.1, 0.5, 0.9, 1.2, 1.4, 1.6, 1.8, 3.3$, and 3.7; $Y_2(0)/\pi = 0.5$. Smaller arrows on the trajectories are drawn at intervals $\Delta t = 2.0$.

Up to $W = 1.8$ at least, particles accumulate on the cell walls for either value of R. For $W = 2.0$, the aerosol particles ($R = 0$) still accumulate on the cell walls, as shown by the particle position plot of Fig. 10(a), at $t = 80$. For $R = 0.4$, however, the particles are scattered throughout the cells with no apparent structure. Figure 10(b) shows the position plot at $t = 80$. At $t = 160$ (not shown) it is equally disorganized. A check of individual trajectories, and in particular of the values of Y and V as the trajectories cross cell boundaries in the x_2 direction, confirms this lack of asymptotic merging of the trajectories in this case. Why this change in behavior takes place is not clear and no explanation is offered here save to note that it is an effect of the increased added mass, which, as noted in Sec. I, acts in opposition to the inertia of the particle.

Finally, it is interesting to compare the average particle settling velocity $\langle V_2 \rangle$ for the two different values of R, $R = 0$ and $R = 0.4$. This may be found by evaluating $V_2(t)$ for a large number of particles initially distributed uniformly through the cells and averaging over all the particles. Alternatively, where the particle trajectories merge into an asymptotic path it is sufficient to compute a single trajectory far enough so that it has reached the asymptotic, periodic form and then evaluate the time taken to cross two or four cells in the x_2 direction, depending on the asymptotic periodicity. Figure 11 shows the computed average settling velocity $\langle V_2 \rangle$ for both values of R. Note that in the absence of particle inertia, particles remain uniformly distributed so that $\langle V_2 \rangle = W$.

When $A = 2$ and $R = 0$, the graph of $\langle V_2 \rangle$ goes through several transitions that coincide with the local minima or maxima of $\langle V_2 \rangle$. For $W \leqslant 0.17$ the asymptotic particle trajectories are not confined to a single vertical column of cells, but go at 45° to the vertical on either side of the vertical. The trajectories have a periodicity of one cell vertically by one cell horizontally. Above $W = 0.18$ the particles settle vertically, with a period of two cells in the x_2 direction. Between $W = 0.675$ and $W = 0.7$ there is another transition where the period in the x_2 direction becomes four cells. For $W \geqslant 1$, the particles settle along the vertical cell boundaries, experiencing successively upflow and downflow regions. The upflow significantly reduces the settling velocity. Indeed, for $W = 1$ the trajectory passes through an equilibrium point which is neutrally stable and $\langle V_2 \rangle$ essentially drops to zero. As W becomes large, the flow field has decreasing influence on settling and eventually $\langle V_2 \rangle$ is approximately the same as W.

When $A = 2$ and $R = 0.4$ we do not have the same transitions. The particles settle in a single vertical column of cells, with a period of two cells in the x_2 direction. Again, for

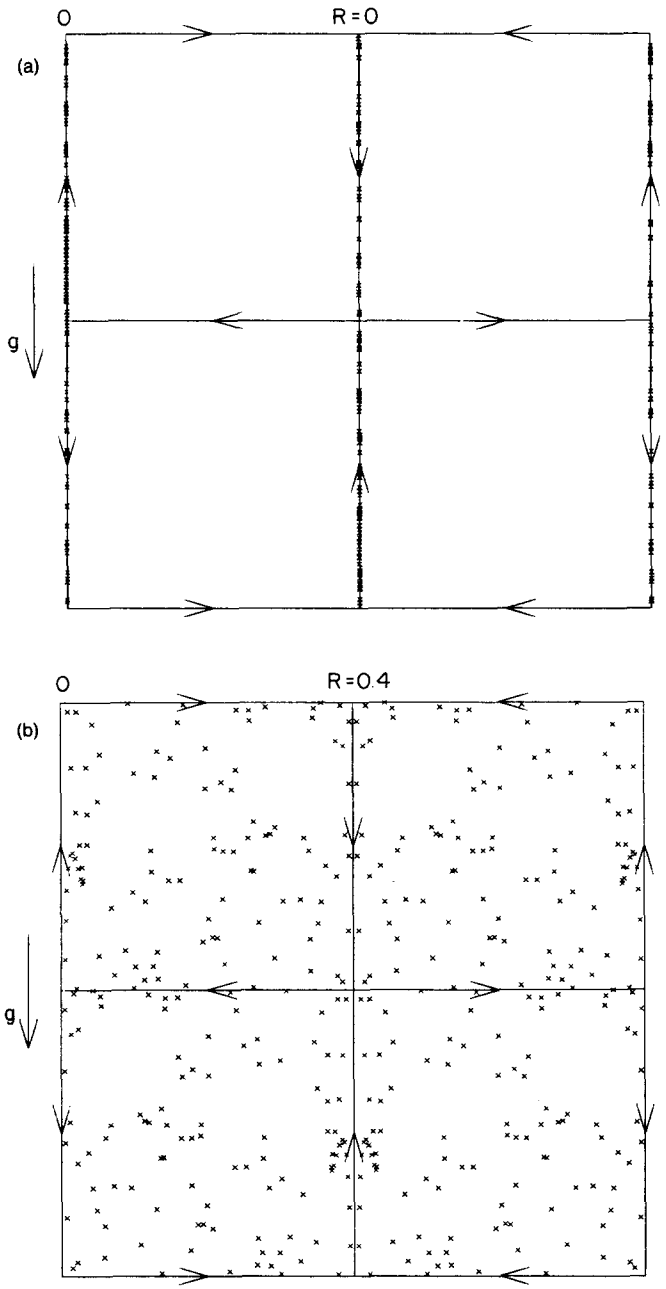

FIG. 10. Particle position plots at $t = 80$ for particles with inertia parameter $A = 2$, still-fluid settling velocity $W = 2.0$: (a) mass ratio parameter $R = 0$; (b) 0.4.

W greater than about 1 the particles collect along the vertical boundaries and the settling velocity $\langle V_2 \rangle$ is reduced by the upflow regions. An equilibrium point exists for $W = 1.02$, and while it is unstable, the growth rates are so small that it is close to being neutrally stable.

The general conclusions from these and other computations are first, that for particles significantly denser than the surrounding fluid, particle suspension does not occur. Second, the asymptotic merging of trajectories into isolated paths is a general feature that is not sensitive to the value of R within this range. Finally, the average settling velocity of the particles is greater than that in still fluid if the still-fluid settling velocity W is small, but is significantly reduced when the value of W approaches 1.

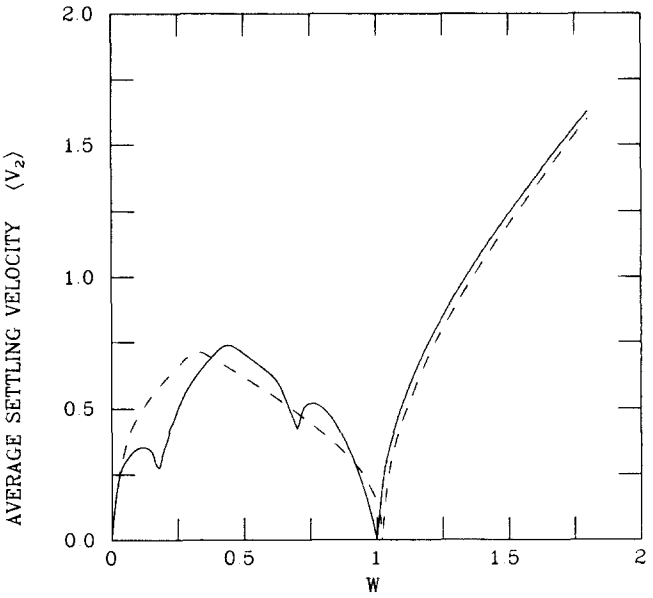

FIG. 11. Average particle settling velocity $\langle V_2 \rangle$ against still-fluid settling velocity W for $A = 2$: —, $R = 0.0$; ----, $R = 0.4$.

V. BUBBLE LIMIT: $R=2$

The stability analysis in Sec. III indicates that for bubble particles stable equilibrium points exist which may lead to the permanent suspension of the particles. To test this possibility, some sample trajectories have been computed for bubble particles $R = 2$, and for a still-fluid, bubble rise speed Q of 0.5; see Fig. 12(a). The inertia parameter of the bubble B is set equal to 10.0, the same as for the stability diagram in Fig. 4. Six of the particles released spiral in toward interior equilibrium points and never escape from their initial cell, while a seventh particle is trapped after passing through two cells. The two particles that do rise through the cells zigzag through the upflow regions of each cell, rising faster than in still fluid. In contrast, Fig. 12(b) shows the particle trajectories for $Q = 1.25$. Here there are no equilibrium points and all the particles escape, rising rapidly through the upflow regions of each cell.

The particle position diagram for $Q = 0.5$, Fig. 13, shows the corresponding positions of an initially uniform array of particles at $t = 20$, the time at which the computations in Fig. 12 were stopped. There is a strong clustering of particles about the equilibrium points, and if the computations are continued further it is found that 90% of the particles spiral in toward these points and are trapped. The particle position plots can also be used to find the long-term asymptotic form of the particle motion and whether or not bubble particles exhibit the same merging of trajectories found for aerosol particles. The long-term behavior for $Q = 1.25$ is shown in Fig. 14(a). All the particles here have collected along simple, well-defined curves that pass through the central region of each cell and are biased toward the upflow region of each cell. The merging of trajectories into isolated paths thus still occurs. But the accumulation for rapidly rising bubbles is between vertical cell boundaries, as opposed to on the boundaries as found for rapidly settling aerosol particles. Figure 14(b) gives the asymptotic behav-

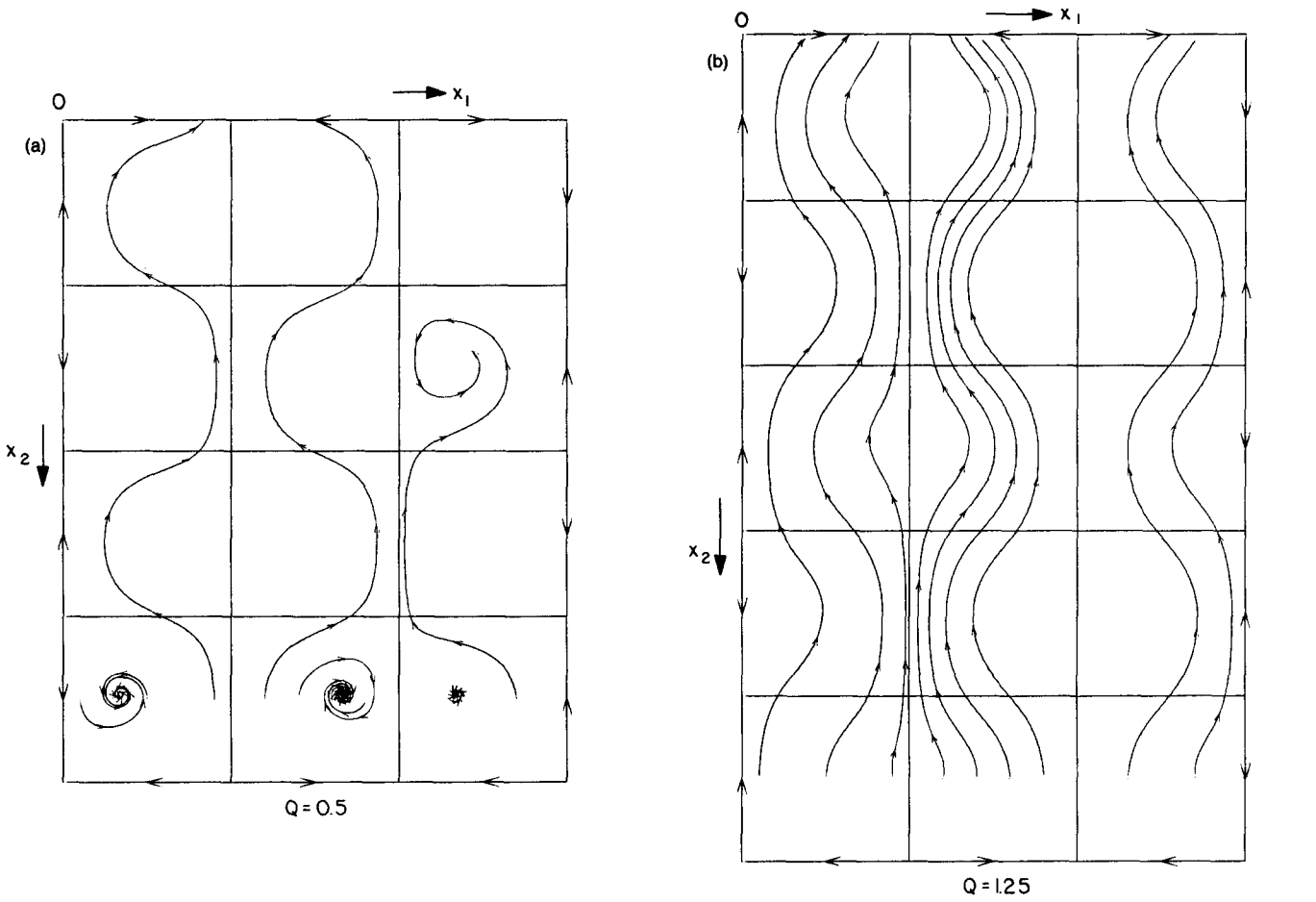

FIG. 12. Particle trajectories for bubbles, $R = 2$, rising through the cellular flow field due to buoyancy forces: (a) still-fluid bubble rise velocity $Q = 1.25$; (b) $Q = 0.5$. Bubble inertia parameter $B = 10.0$; initial particle positions are as in Fig. 6, but with $Y_2(0)/\pi = 4.5$ in (a) and $Y_2(0)/\pi = 3.5$ in (b). The smaller arrows are drawn on the trajectories at time intervals $\Delta t = 2$ up to $t = 20$.

ior for $Q = 0.8$. In this instance there are both stable equilibrium points, as marked by the isolated cross marks, and isolated accumulation curves. Although these stable equilibrium points appear as single marks in the diagrams, they each in fact represent some 20 particles that have been trapped there.

The general picture that emerges is that for Q large enough so that no equilibrium points exist, the particles accumulate along a simple isolated curve, as in Fig. 14(b). For small values of Q less than about 0.4, the effect of the stable equilibrium points dominates and all the particles are trapped, held in suspension by the flow at these isolated points. For intermediate values of Q, a combination of these two responses occurs with more and more particles trapped as Q decreases, and less rising along the isolated asymptotic path. The fraction of particles suspended in the flow as Q varies is given in Fig. 15, as is the average particle rise velocity $-\langle V_2 \rangle$. This observation that increasingly more particles are suspended as Q decreases is consistent with the results of Auton[7] and of Thomas *et al.*,[8] who studied the motion of bubbles in the irrotational flow caused by a uniform vortex cylinder or line vortex and found that as the strength of the vortex increased, particles over a wider area would be drawn in toward the equilibrium point and trapped. The equation of particle motion that Auton[7] and Thomas *et al.*[8] used, however, was somewhat different from

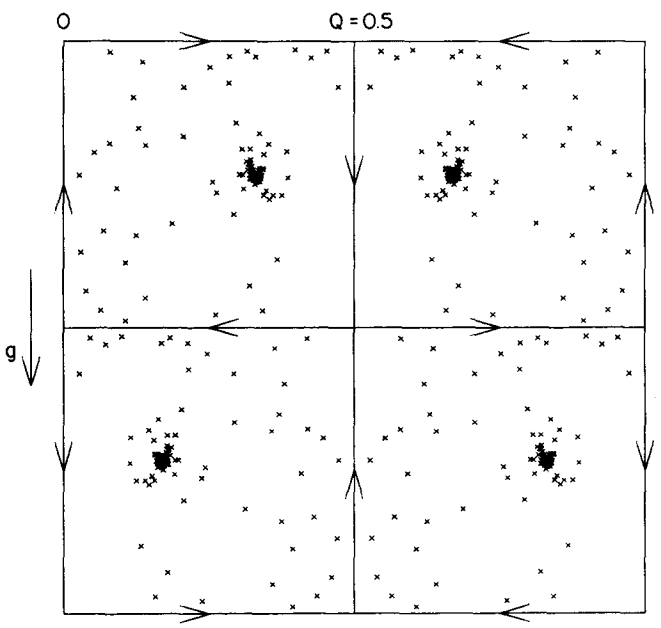

FIG. 13. Particle position plot at $t = 20$ for bubbles, $R = 2.0$, with inertia parameter $B = 10$ and still-fluid rise velocity $Q = 0.5$.

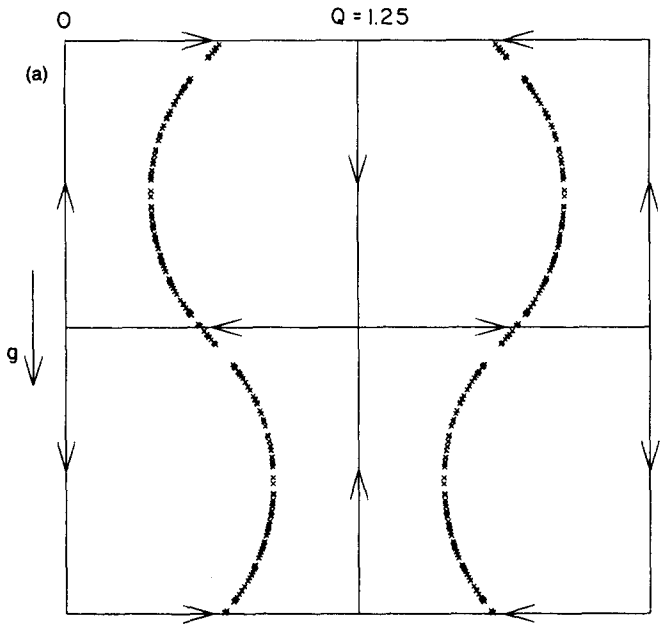

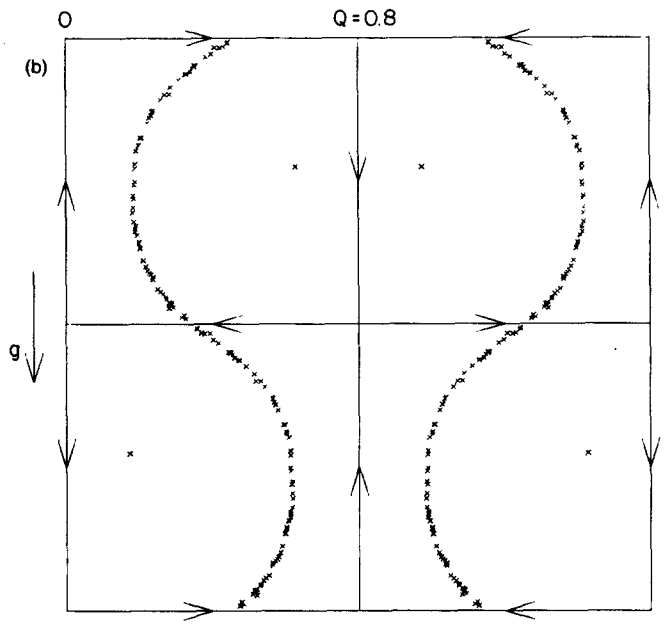

FIG. 14. Particle position plots for bubbles, $R = 2$, showing the long-term accumulation: (a) $Q = 1.25$ and $t = 80$; (b) $Q = 0.8$ and $t = 100$. Inertia parameter $B = 10$.

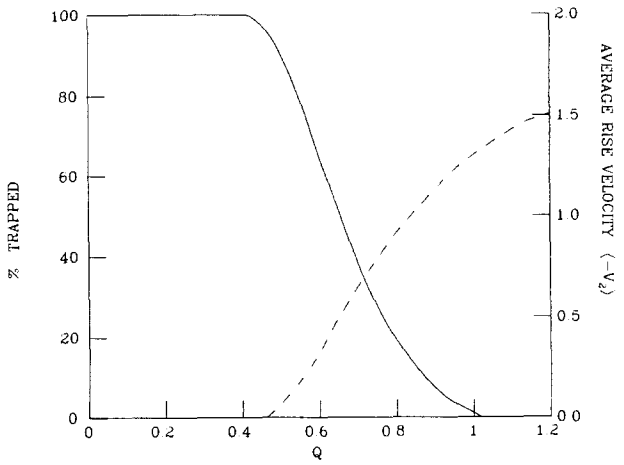

FIG. 15. Percentage of bubbles suspended at the equilibrium points (solid curve) and the average particle rise velocity $\langle -V_z \rangle$ (dashed curve) averaged over all particles as the still-fluid rise velocity Q is varied. Inertia parameter $B = 10$ and mass ratio parameter $R = 2$.

(16) and was based on a large particle Reynolds number, as opposed to the Stokes flow regime assumed here.

VI. TRANSITION RANGE: $0.4 < R < 2$

As the mass ratio parameter R varies between 2 and 0.4 a transition takes place between the "bubble" response described in Sec. V and the "aerosol" response described in Sec. IV. Particles less dense than the surrounding fluid $R > \frac{2}{3}$ exhibit much the same type of motion as found for the bubbles. Particles either accumulate along an isolated curve passing through the central region of each cell, rising continuously, or else are trapped at some stable equilibrium point. Again, in this range it is appropriate to use the parameters B and Q and assign fixed values to these as R is varied. The particle position diagram, Fig. 16, shows the particle accumulation for $B = 5$ and $Q = 1.25$ when R is 1.0. Here the corresponding value of W is -0.625. Particles are concentrated at the stable equilibrium points or else collect along isolated accumulation curves. The accumulation process takes longer than for $R = 2$, but is similar for the same value of W. Eventually 49% of the particles are suspended by the equilibrium points and the accumulation curve becomes more sharply defined.

As R approaches the value of $\frac{2}{3}$, a transition takes place. The value of the actual still-fluid settling velocity W goes to zero for any fixed value of Q and the equilibrium points in the cells become unstable for R less than $\frac{2}{3}$. Figure 17(a) is a

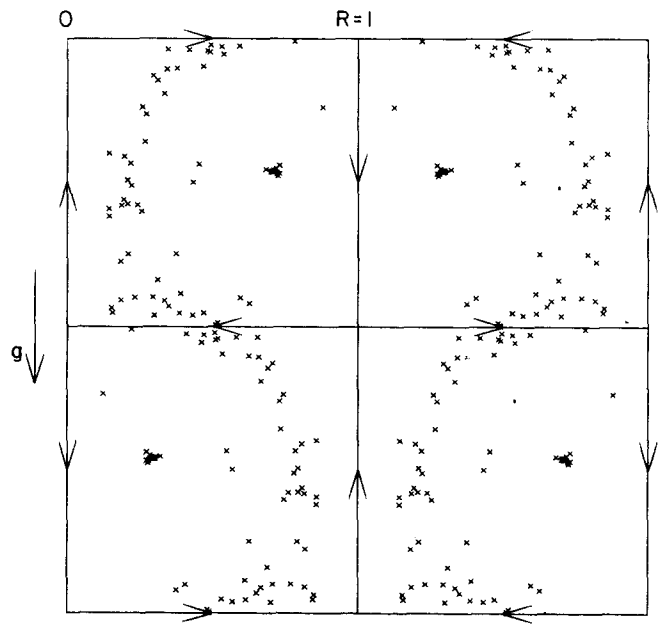

FIG. 16. Particle position plot $t = 100$ for particles less dense than the surrounding fluid $R = 1.0$. Inertia parameter $B = 10$, $Q = 1.25$, and the corresponding value of $W = -0.625$.

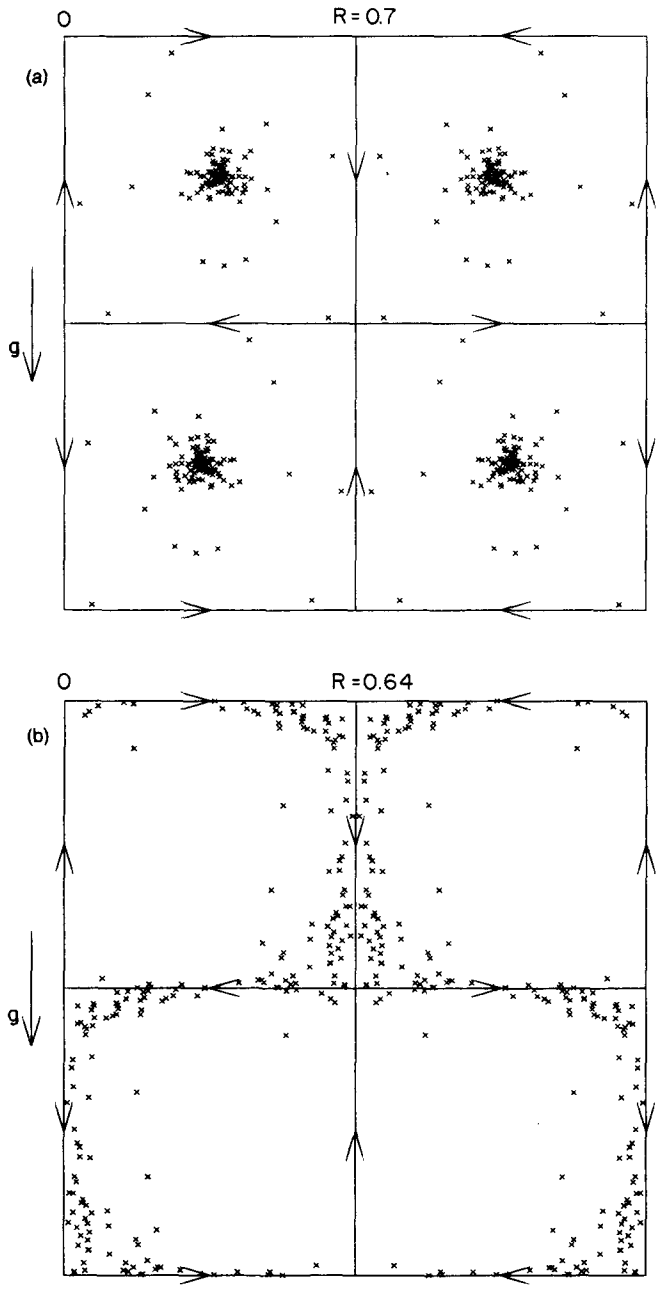

FIG. 17. Particle position plots at $t = 200$: (a) particles less dense than the fluid, $R = 0.70$; (b) particles denser than the fluid, $R = 0.64$. Inertia parameter $B = 10$ and $Q = 1.25$.

long-term particle position plot for $R = 0.7$ just above the transition value. The value of W is about -0.09. The equilibrium points are stable and for this low value of W all the particles are eventually trapped at these points. Figure 17(b), on the other hand, shows the particle positions for $R = 0.64$ just below the transition value. The corresponding value of W is $+0.078$. No particle suspension occurs and the particles accumulate, albeit slowly, along isolated curves passing through the downflow region of each cell. This is essentially the response found for the aerosol range $R \leqslant 0.4$.

Other values of Q may be tested, but all seem to demonstrate the same features. For any finite value of Q, the transition takes place at $R = \frac{2}{3}$: For $R > \frac{2}{3}$ the response is bubble-like, and for $R < \frac{2}{3}$ it is aerosol-like.

VII. CONCLUDING REMARKS

The preceding results show clearly that the long-term accumulation of particles in a cellular flow is a general feature not confined to aerosol particles, but applicable to particles of arbitrary density compared to that of the fluid. The accumulation may be an asymptotic merging of individual particle trajectories into some isolated path through the cells, or it may be an accumulation at some equilibrium point. The critical feature that is important is the inertia of the particles or the inertia of the fluid, in the case of bubbles. It is this aspect that distinguishes the particle motion found here from the results given by Stommel,[1] where, as illustrated by Fig. 7, there is no tendency for particles to accumulate in the absence of inertia. Where the particles do accumulate along some path this often leads to an increase in the rate at which particles pass through the cells.

From a mathematical viewpoint this phenomenon is an example of stable attractor sets for a dissipative non-Hamiltonian system.[11] From a physical viewpoint, though, it shows that it is misleading to consider the motion of discrete particles as similar to that of Lagrangian fluid elements, especially in a steady flow. The concentration of particles preferentially in one region of the flow field compared to another can influence not only particle settling velocities, but also the dispersion of particles or particle coagulation. In an unsteady flow or a turbulent flow it is unlikely that the same degree of ordered structure will develop, but a tendency for particles to concentrate in certain regions will still persist.

Some insight into this accumulation process may be gained by considering the effect of weak inertia. The equation of particle motion (16), as used here, may be approximated for large values of A, the inertia parameter, as

$$\mathbf{V}(t) = \mathbf{u}(\mathbf{Y},t) + \mathbf{W} - \frac{1}{A}\frac{d}{dt}(\mathbf{u}(\mathbf{Y},t) + \mathbf{W}) + \frac{R}{A}\left(\frac{3}{2}\mathbf{u} + \frac{1}{2}\mathbf{W}\right)\cdot\nabla\mathbf{u} + O\left(\frac{1}{A^2}\right), \tag{38}$$

where the inertia terms have been estimated by setting $\mathbf{V}(t)$ equal to $\mathbf{u}(\mathbf{Y},t) + \mathbf{W}$ as a first approximation. This allows the particle velocity to be specified completely by its instantaneous position $\mathbf{Y}(t)$, and (38) may be written in terms of a "particle flow" field $\mathbf{v}$:

$$\mathbf{V}(t) = \mathbf{v}(\mathbf{Y}(t),t), \tag{39}$$

$$\mathbf{v}(\mathbf{x},t) = \mathbf{u}(\mathbf{x},t) + \mathbf{W} - \frac{1}{A}\left(\frac{\partial\mathbf{u}}{\partial t} + (\mathbf{u} + \mathbf{W})\cdot\nabla\mathbf{u}\right) + \frac{R}{A}\left(\frac{3}{2}\mathbf{u} + \frac{1}{2}\mathbf{W}\right)\cdot\nabla\mathbf{u}. \tag{40}$$

Even if the flow field $\mathbf{u}(\mathbf{x},t)$ is incompressible, the "particle flow" field $\mathbf{v}$ will be compressible:

$$\nabla\cdot\mathbf{v} = \frac{1}{A}\left(\frac{3}{2}R - 1\right)\left(\frac{\partial u_i}{\partial x_i}\frac{\partial u_i}{\partial x_j}\right) \tag{41}$$

and

$$\frac{\partial u_j}{\partial x_i}\frac{\partial u_i}{\partial x_j} = \frac{1}{4}\left(\frac{\partial u_i}{\partial x_j} + \frac{\partial u_j}{\partial x_i}\right)^2 - \frac{1}{4}\left(\frac{\partial u_i}{\partial x_j} - \frac{\partial u_j}{\partial x_i}\right)^2. \tag{42}$$

The divergence of $\mathbf{v}(\mathbf{x},t)$ for aerosol particles, $R < \frac{2}{3}$, is posi-

tive in regions of strong vorticity and negative where the strain rate is dominant. Thus during the motion of such particles, aerosol particles may be expected to concentrate in regions of high strain rate or low vorticity. For bubble particles, $R > \frac{2}{3}$, the opposite bias should hold.

In the cellular flow field example the strain rate is greatest near the corners of each cell, while the vorticity is largest near the center of each cell. These comments are then consistent with the general observation that rapidly settling aerosol particles collect along the cell boundaries and rapidly rising bubbles accumulate along paths passing through the central portion of each cell. These arguments further generalize the description of the change of stability characteristics for the equilibrium points given in Secs. I and III. These comments, however, are not restricted to the cellular flow problem and should apply in a general context.

ACKNOWLEDGMENTS

This paper is a continuation of the work reported in Maxey and Corrsin.[3] I am indebted to Professor Stanley Corrsin for encouraging me to pursue this work and for his helpful comments.

The author gratefully acknowledges the support of the National Science Foundation through Grant No. ATM-8310136.

[1]H. Stommel, J. Marine Res. **8**, 24 (1949).
[2]B. D. Marsh and M. R. Maxey, J. Volcanol. Geotherm. Res. **24**, 95 (1985).
[3]M. R. Maxey and S. Corrsin, J. Atmos. Sci. **43**, 1112 (1986).
[4]I. R. Wood and B. S. Jenkins, *International Symposium on River Mechanics*, 9–12 January 1973, Bangkok, Thailand (IAHR, Delft, The Netherlands, 1973), Paper A38, pp. 431–442.
[5]M. J. Manton, Boundary Layer Meteorol. **6**, 487 (1974).
[6]P. Nielsen, J. Geophys. Res. **89**, 616 (1984).
[7]T. R. Auton, Ph. D. thesis, University of Cambridge, 1981.
[8]N. H. Thomas, T. R. Auton, K. Sene, and J. C. R. Hunt, *International Conference on Physical Modeling of Multi-Phase Flow*, 19–21 April 1983, Coventry, England (BHRA Fluid Engineering, Bedford, 1983), Paper E1, pp. 169–184.
[9]M. R. Maxey and J. J. Riley, Phys. Fluids **26**, 883 (1983).
[10]R. Clift, J. R. Grace, and M. E. Weber, *Bubbles, Drops, and Particles* (Academic, New York, 1978), p. 35.
[11]J. Guckenheimer and P. Holmes, *Nonlinear Oscillations, Dynamical Systems, and Bifurcations of Vector Fields* (Springer, New York, 1983), p. 33.